

2

3 **Evaluation of Solar Cell Using Terahertz Time-**

4 **Domain Spectroscopy**

5

6

7

8

9 **ABSTRACT**

10

Terahertz time-domain spectroscopy (THz-TDS) has been used to investigate the optical properties of mono silicon solar cell. The sample was optically excited using continuous-wave (CW) light of wavelengths of 800 nm and 365 nm, and the carrier density and mobility were extracted from the THz-TDS data by fitting with the simple Drude model. The conductivity shows nonlinear increase with the optical excitation power. The mobility of the photo-excited carriers also increases nonlinearly with the CW light power. However, the mobility shows tendency to saturate with the increase of illumination power, which can be explained by carrier trapping effect to the impurity states existing in the band-gap region of the base material of solar cell. In addition, it is observed that the carrier density and mobility are smaller for 365 nm light illumination due to surface recombination.

11

12 *Keywords: Terahertz spectroscopy, Solar cell, CW light illumination.*

13

14 **1. INTRODUCTION**

15

16 Solar energy is the most promising readily available source of energy. It is often mentioned

17 as a part of the solution to the energy problems. However, increasing the energy conversion

18 efficiency and reducing the cost of production are the major challenges to make solar

19 electricity more competitive with the conventional energy sources [1, 2]. Today most of the

20 solar cells are made of crystalline silicon because of its large abundance on the earth, low

21 cost and high efficiency. The dynamic properties of photo-excited carriers also play an

22 important role on the photovoltaic conversion efficiency of solar cell. Thus, it is important to

23 understand the optical response of photo-excited carriers in solar cell to further improve the

24 cell efficiency. A variety of measurement techniques for the characterization of photovoltaic

25 cells, such as electroluminescence [3], light beam induced current [4] or voltage and current

26 measurements, require electric contacts and can only be performed on the finished

27 photovoltaic cells. On the other hand, a noncontact and nondestructive technique using

28 terahertz (THz) waves is widely utilized on various materials such as semiconductors, liquids

29 and superconductors to obtain a variety of physical properties [5-7]. The benefit of THz

30 technique is that it can be used for the characterization of solar material or semi-finished

31 solar cells without electric contacts at the beginning as well as during the production process

32 of photovoltaic cells. By employing this technique, a wide variety of research, such as

33 spectroscopic [8], imaging [9] and terahertz emission [10] have been done on investigation

34 of solar cells and related materials. It was effectively applied to study the properties of

35 irradiated silicon wafer for space solar cell application [8]. In our previous study, we used a

36 laser terahertz emission microscope technique to study THz emission from a silicon solar

37 cell and visualize the temporal photo-current generated by femtosecond laser pulse

38 illumination [10]. We also used this technique to examine both the effects of optically

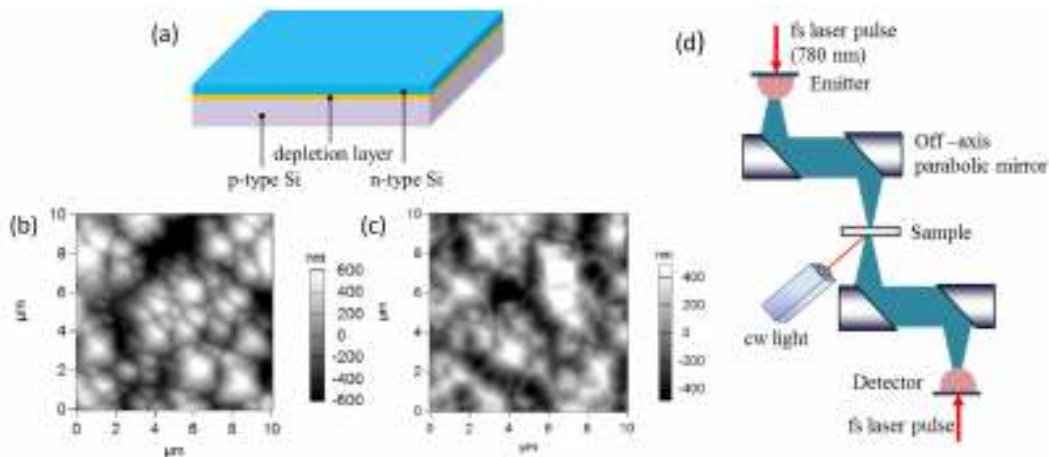
39 generated carriers by a continuous-wave (CW) light illumination and applied bias voltage on

40 the behavior of a solar cell [11]. Another advantage of THz spectroscopy is that the

41 frequency dependent absorption coefficient and refractive index can be obtained from the
42 detected signal. From this the complex dielectric constant and complex conductivity can be
43 determined. After analyzing the conductivity data, we can easily get the carrier transport
44 properties of material, e.g. charge carrier density and mobility. Under illumination, these two
45 parameters are particularly important because they dominate the electrical behavior of solar
46 cell. In this work, we applied transmission-type terahertz time-domain spectroscopy (THz-
47 TDS) to investigate the optical properties and charge carrier dynamics in mono Si solar cell
48 under CW light illumination. In particular, we measured illumination dependence of
49 conductivity, charge carrier density and mobility.
50

51 2. EXPERIMENTAL DETAILS

52
53 The sample used in this study was a commercial mono silicon solar cell (cell without
54 electrodes and antireflection coating) which is configured as a large-area *p-n* junction.
55 Typical doping densities are $1 \times 10^{19} \text{ cm}^{-3}$ in n-type region and $1 \times 10^{16} \text{ cm}^{-3}$ in p-type region
56 and the thickness of the emitter (n-type region) is $\sim 0.5 \mu\text{m}$ [12]. The overall thickness of the
57 sample was $182 \mu\text{m}$ measured by THz peak delay technique [13]. The schematic structure
58 of the solar cell and its AFM images are shown in Fig. 1(a)-1(c). The front surface image in
59 Figure 1(b) showed that the several pyramidal structures with different sizes are randomly
60 distributed over the entire surface. These shapes play an important role in improving light
61 coupling into solar cells. The root mean square (rms) average roughness value was 150 nm .
62 On the other hand the rear surface is an unpolished rough surface as shown in Figure 1(c).
63 The rms average roughness value was 240 nm , which is higher than that of front surface.
64 The experimental setup used for THz-TDS measurement is also shown schematically in
65 Figure 1(d). A femtosecond (fs) laser with the center wavelength of 780 nm is used for the
66 excitation of low-temperature-grown GaAs (LT-GaAs) photoconductive antennas which are
67 used for generation and detection of THz pulses. The terahertz radiation was focused onto
68 the sample with a spot diameter of about 5 mm . The sample was illuminated with CW light
69 with wavelengths of 800 nm and 365 nm with area of 0.5 cm^2 and 0.88 cm^2 , respectively.
70 The illumination area is larger than that of terahertz beam spot to ensure uniform
71 illumination. Measurements were carried out on both surfaces of the sample at various
72 illumination powers. All measurements were performed at room temperature with relative
73 humidity of around 30-35%.
74



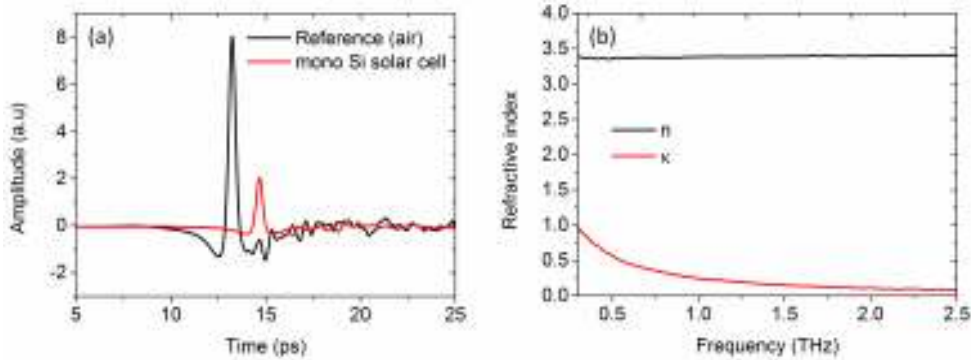
75
76
77
78
79

Fig. 1. (a) Schematic structure of mono Si solar cell and its AFM images of (b) front textured surface (c) rear rough surface. 1(d) Schematic of experimental setup for transmission-type THz-TDS

80 **3. RESULTS AND DISCUSSION**

81

82 Figure 2 (a) shows the waveforms of the THz pulses through the free space and the mono Si
 83 solar cell without CW light excitation. After applying Fast Fourier transform to the time
 84 domain spectra, the complex refractive index can be estimated[14]. The complex refractive
 85 index with real part n and imaginary part κ (extinction coefficient) in the THz frequency
 86 region is shown in Fig 2(b). The real part of the refractive index is related to the speed of
 87 light in the medium, the imaginary part is directly related to the absorption of light through the
 88 material. The average value of refractive index of mono Si solar cell without light excitation is
 89 obtained as 3.39, which is very close to the reported value of 3.41 for crystalline silicon [6].
 90



91

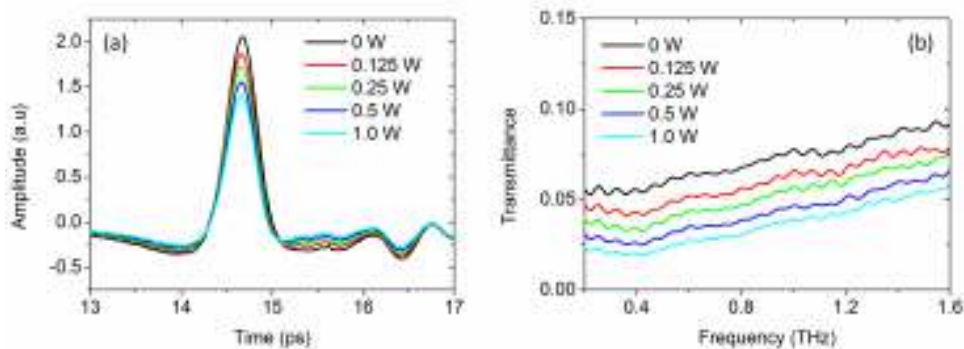
92

93 **Fig. 2.(a) Waveforms of the terahertz pulses of free space and the pulses through**
 94 **mono Si solar cell. (b) Complex refractive index with real part n and imaginary part κ of**
 95 **the cell**

96

97 Figure 3(a) shows the waveforms of the THz pulses transmitted through the solar cell with
 98 illumination of the 800 nm CW laser from front surface at various powers. It is seen that the
 99 amplitude of the terahertz waveforms transmitting through the photo-excited sample is
 100 greatly reduced by the absorption of photo-excited carriers. By using the ratio between
 101 reference and sample waveforms in Fresnel coefficient equations, the transmission can be
 102 estimated[14,15]. The transmittance of the THz wave at various illumination powers is
 103 presented in Fig. 3(b). The terahertz transmission decreases with the illumination power of
 104 CW laser due to increase of photo-excited carriers in the sample.
 105

106



107

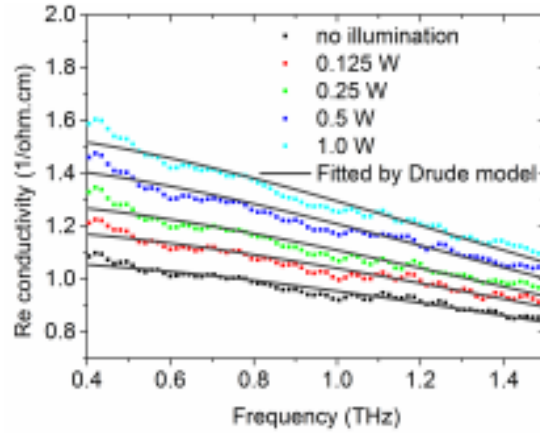
108

109 **Fig. 3. (a) Waveforms of the THz pulses transmitted through the excited **monoSi** solar**
 110 **cell at 800 nm with various illumination powers. (b) Transmittance obtained from the**
 waveforms in (a)

111 The complex conductivity is also obtained from the complex refractive index using $\tilde{n}^2 =$
 112 $\tilde{\epsilon}(\omega) = \epsilon_{Si} + i\tilde{\sigma}(\omega)/\omega\epsilon_0$, where $\tilde{\epsilon}$ is the complex dielectric constant, ϵ_0 is the permittivity of
 113 free space and ϵ_{Si} is the dielectric constant of undoped silicon [15]. Figure 4 shows
 114 frequency dependence of experimental data and the calculation of real part of conductivity of
 115 the solar cell with front illumination at 800 nm with various powers. The real part of the
 116 conductivity decreases with increasing frequency in the THz range. It is also evident that the
 117 conductivity increases with the illumination power of CW laser. The frequency dependence
 118 of the conductivity can be well described with the simple Drude model [16]. According to the
 119 Drude model, the complex conductivity is expressed as
 120

$$\tilde{\sigma}(\omega) = \frac{\sigma_{dc}}{1 - i\omega\tau}$$

121
122



123
124
125
126
127

Fig. 4. Real part of conductivity of mono Si solar cell at 800 nm with various illumination powers from front surface; the solid lines are fitted curves with simple Drude model

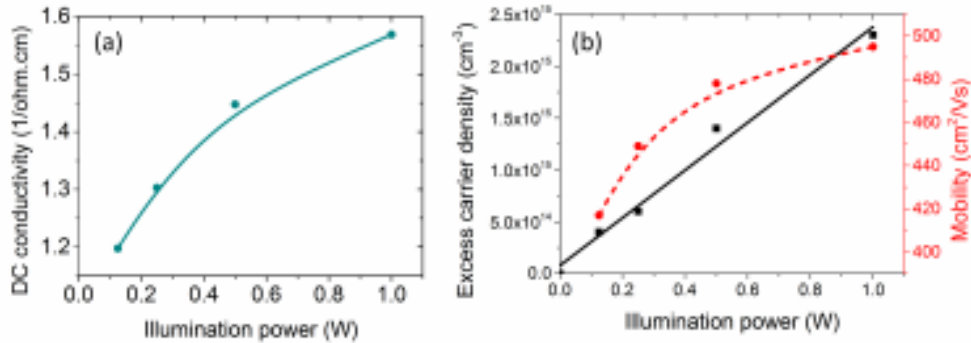
128 where σ_{dc} is the DC conductivity, τ is the average carrier scattering time. Solid lines in figure
 129 4 are fitting lines to the real part of conductivity at each level of illumination power using the
 130 simple Drude model. The fitting parameters DC conductivity σ_{dc} and carrier scattering time τ
 131 are extracted from the fitted curves and presented in Table 1. The carrier density $N =$
 132 $\sigma_{dc}m^*/e^2\tau$ and the mobility $\mu = e\tau/m^*$ are calculated by using the fitting parameters of σ_{dc}
 133 and τ with the effective mass $m^* = 0.26m_0$ for silicon [16].
 134

135 **Table 1. Fitting parameters based on simple Drude model under various illumination**
 136 **powers. The columns present the values for illumination power (mW), the DC**
 137 **conductivity σ_{dc} (1/ Ω cm) and the carrier scattering time τ (ps) extracted from the**
 138 **fitted curves; the excess carrier density N (cm^{-3}) and the mobility μ (cm^2/Vs)**
 139 **determined by σ_{dc} and τ .**
 140

800 nm					365 nm				
Power	σ_{dc}	τ	N	μ	Power	σ_{dc}	τ	N	μ
125	1.20	0.0618	4.0×10^{14}	417	100	1.096	0.0579	2.0×10^{14}	392
250	1.30	0.0665	6.0×10^{14}	449	200	1.107	0.0588	1.0×10^{14}	398
500	1.45	0.0708	1.4×10^{15}	478	300	1.113	0.0575	5.0×10^{14}	389

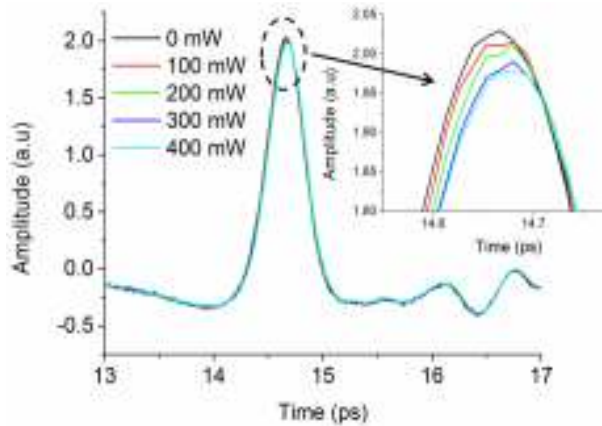
141
142
143
144
145
146
147
148
149
150
151
152
153
154
155
156

The DC conductivity, excess carrier density and mobility are plotted in Figure 5 as a function of the illumination power. It is shown in Fig. 5(a) that the DC conductivity rises nonlinearly with the illumination power of CW laser and tends to saturate with the increase of illumination power. It is also found in Fig. 5(b) that the excess carrier density increases linearly and, the mobility increases and tends to saturate with the illumination power of CW laser. This tendency to saturate in mobility may be explained by the saturation effect of photo-excited carrier trapping in the impurity states in the band-gap of the solar cell [17-21]. Minority carrier traps are often present in the solar grade crystalline silicon [19, 20]. Due to laser illumination, electron-hole pairs are generated in the base (p-type) of the solar cell. A part of minority electrons would be captured or scattered by impurity states which temporarily hold electrons. As the illumination power increases, these states progressively trap electrons and become neutral. Therefore, the capture and scattering cross sections for electrons are reduced significantly with increasing excess carrier density, which increases the mobility of minority carriers.



157
158
159
160
161
162

Fig. 5. 800 nm laser illumination power dependence of (a) DC conductivity and (b) excess carrier density and mobility deduced from the simple Drude model fitted to the real conductivity

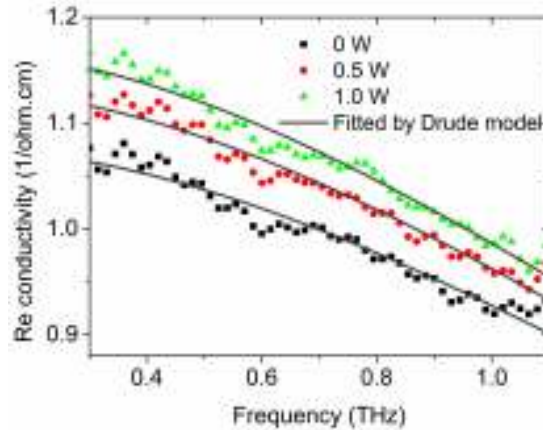


163
164
165
166
167
168

Fig. 6. Waveforms of the THz pulses transmitted through the excited monoSi solar cell at 365 nm with various illumination powers

We also carried out similar measurements under 365-nm light illumination. Figure 6 shows the waveforms of the THz pulses transmitted through the solar cell with illumination of the

169 365 nm light at various powers. The amplitude of the THz waveforms decreases very small
 170 with the illumination power. After analyzing the waveforms data, the excess carrier density
 171 and mobility are calculated and also presented in Table 1. The excess carrier density is
 172 smaller for illumination at 365 nm than that for 800 nm. This can be explained by considering
 173 the penetration depth of 365 nm light. The penetration depth in silicon for 365 nm is about
 174 0.01 μm [22]. Under 365 nm light illumination, the photo-excited carriers are generated
 175 within 10 nm from the surface of the solar cell and their lifetime strongly affected by the high
 176 surface recombination.
 177



178
 179
 180 **Fig. 7. Real part of conductivity of mono Si solar cell at 800 nm with various**
 181 **illumination powers from rear surface; the solid lines are fitted curves with simple**
 182 **Drude model**
 183

184 More measurements also performed with illumination at 800 nm from rear surface of the
 185 solar cell. In these measurements the THz pulse are transmitted from the back surface to the
 186 front surface of the solar cell. Figure 7 shows the real part of conductivity data fitted with the
 187 simple Drude model. From the fitting parameters the excess carrier density and mobility are
 188 calculated. The calculated excess carrier densities are 1×10^{14} and $2 \times 10^{14} \text{ cm}^{-3}$ and the
 189 mobility are 455 and 466 cm^2/Vs for 0.5 and 1.0 W illumination, respectively. From these
 190 results it is seen that the carrier density and mobility increase with increasing illumination
 191 power, which are similar to the front illumination results. However, the value of carrier
 192 density and mobility are smaller than those of the front illumination results. For example, at 1
 193 watt illumination the carrier density and mobility are decreased by 21% and 5.9%,
 194 respectively, compared to the front illumination results. This is because the reflectance of
 195 rear surface is much larger than that of textured front surface [23]. Textured front surface
 196 reduces the reflection of CW laser and generated more photo carriers. Moreover, the
 197 unpolished rear surface recombination is thought to be higher than that of the front surface
 198 because it contains a large number of defects and impurities that act as a recombination
 199 centers.
 200

201 4. CONCLUSION

202
 203 We have employed transmission-type THz-TDS system to measure optical properties of
 204 mono Si solar cell during photo-excitation by 800nm and 365nm CW light. The terahertz
 205 transmission is greatly reduced by the absorption of photo-excited carriers generated by the
 206 800nm CW laser illumination. The analysis of transmission data yields complex refractive
 207 index as well as conductivity. The conductivity data can be fitted with the simple Drude
 208 model and from the fitting results the excess carrier density and mobility are deduced. The

209 carrier mobility increases and saturated with the illumination of CW laser. This phenomenon
210 is explained by the effect of carrier trapping in the impurity states in the band gap of solar
211 cell. We also observed small effect under 365nm light illumination due to the high surface
212 recombination.

213

214

215 **ACKNOWLEDGEMENTS**

216

217 Authors would like to thank Mr. Hidetoshi Nakanishi, Dainippon Screen Mfg. Co. for
218 providing us the mono silicon solar cell.

219

220 **REFERENCES**

221

222 1. Choubey PC, Oudhia A and Dewangan R. A review: Solar cell current scenario and
223 future trends. Recent Research in Science and Technology. 2012;4(8):99-101.

224 2. Saga Tatsuo. Advances in crystalline silicon solar cell technology for industrial mass
225 production. NPG Asia Mater. 2010;2(3):96-102.

226 3. Fuyuki T and Kitiyanan A. Photographic diagnosis of crystalline silicon solar cells
227 utilizing electroluminescence. Appl Phys A. 2009;96:189-196.

228 4. Thantsha NM, Macabebe EQB, Vorster FJ, Van Dyk EE. Opto-electronic analysis of
229 silicon solar cells by LBIC investigations and current-voltage characterization. Physica
230 B. 2009;404:4445-4448.

231 5. Tonouchi M. Cutting-edge terahertz technology. Nature Photonics. 2007;1:97-105.

232 6. Grischkowsky D, Keiding S, Exter M, and Fattinger C. Far-infrared time-domain
233 spectroscopy with terahertz beams of dielectrics and semiconductors. J. Opt. Soc. Am.
234 B. 1990;7(10):2006-2015.

235 7. Pedersen JE and Keiding SR. THz time-domain spectroscopy of nonpolar liquids. IEEE
236 Journal of Quantum Electronics. 1992;28:2518-2522.

237 8. Nagai N, Sumitomo M, Imaizumi M, and Fukasawa R. Characterization of electron- or
238 proton-irradiated Si space solar cells by THz spectroscopy. Semicond. Sci. Technol.
239 2006;21:201-209.

240 9. Minkevičius L et al. Solar cell imaging and characterization by terahertz techniques.
241 Proc. of SPIE. 2012;8496:8496131-6.

242 10. Nakanishi H, Fujiwara S, Takayama K, Kawayama I, Murakami H, and Tonouchi M.
243 Imaging of a polycrystalline silicon solar cell using a laser terahertz emission
244 microscope. Appl. Phys. Express. 2012;5:112301.

245 11. Salek KA, Nakanishi H, Ito A, Kawayama I, Murakami H, and Tonouchi M. Laser
246 terahertz emission microscopy studies of a polysilicon solar cell under the illumination of
247 continuous laser light. Optical Engineering. 2014;53(3):0312041-6.

248 12. Nelson J. The Physics of Solar Cells, London:Imperial College Press;2003.

249 13. Jen C-Y and Richter C. Sample thickness measurement with THz-TDS: Resolution and
250 Implications. J Infrared MilliTerahz Waves. 2014;35:840-859.

251 14. Lee Y-S. Principles of Terahertz Science and Technology (chapter 2). New York:
252 Springer;2009.

253 15. Sakai K (Ed.). Terahertz Optoelectronics (pp. 203-212). Berlin:Springer;2005.

254 16. Exter M and Grischkowsky D. Carrier dynamics of electrons and holes in moderately
255 doped silicon. Phys. Rev. B. 1990;41:12140-12149.

256 17. Fabre E, Mautref M and Mircea A. Trap saturation in silicon solar cells. Applied Physics
257 Letters. 1975;27(4):239-241.

258 18. Fan HY. Effect of traps on carrier injection in semiconductors. Physical review. 1953;92
259 (6)1424-1428.

260 19. Macdonald D and Cuevas A. Trapping of minority carriers in multicrystalline silicon.
261 Appl. Phys. Lett. 1999;74(12):1710-1712.

- 262 20. Schmidt J and Cuevas A. Electronic properties of light-induced recombination centers in
263 boron-doped Czochralski silicon. *J. Appl. Phys.* 1999;86(6):3175-3180.
- 264 21. Macdonald D, Kerr M and Cuevas A. Boron-related minority-carrier trapping centers in
265 p-type silicon. *Appl. Phys. Lett.* 1999;75(11):1571-1573.
- 266 22. Aspnes DE and Studna AA. Dielectric functions and optical parameters of Si, Ge, GaP,
267 GaAs, GaSb, InP, InAs, and InSb from 1.5 to 6.0 eV. *Phys. Rev. B.* 1983;27(2):985-
268 1009.
- 269 23. Barrio R, González N, Cárabe J, Gandía JJ. Optimisation of NaOHtexturisation process
270 of silicon wafers for heterojunction solar-cells applications. *Solar energy.* 2012;86:845-
271 854.